1-1-2020

Autonomous Control Strategy for Microgrid Operating Modes Smooth Transition

Yaran Li

Long Fu

Ke Meng

Zhao Dong

Kashem M. Muttaqi
University of Wollongong, kashem@uow.edu.au

See next page for additional authors

Autonomous Control Strategy for Microgrid Operating Modes Smooth Transition

Abstract

© 2013 IEEE. Microgrid transition between standalone and grid-connected modes is a promising alternative to provide the grid with increasing flexibility and availability. However, transition smoothness relies heavily on control topologies and corresponding parameters, which thus remains challengeable. Existing microgrid transition strategies have two major deficiencies: 1) Inverter control mode alters subjected to microgrid operating mode, for instance, the inverter in current control will switch to voltage control when microgrid disconnects to the utility grid; 2) Controller parameters are selected based on practice and experience, where a systematic and efficient approach does not exist. Motivated by these limitations, in this paper, an autonomous control strategy is proposed for microgrid smooth state transitions. It is highlighted in the following aspects: 1) The cascaded control strategy enables smooth state transition within a single control structure, which permits controller independent of mode switching; 2) Nonlinear-Simplex based algorithm is interfaced with electromagnetic transient simulations, searching for optimal controller parameters in order to minimize voltage deviation in a chain of microgrid events. The effectiveness of the control framework is validated with simulations in PSCAD/EMTDC and RTDS.

Publication Details

Y. Li, L. Fu, K. Meng, Z. Dong, K. Muttaqi & W. Du, "Autonomous Control Strategy for Microgrid Operating Modes Smooth Transition," IEEE Access, vol. 8, pp. 142159-142172, 2020.

Authors

Yaran Li, Long Fu, Ke Meng, Zhao Dong, Kashem M. Muttaqi, and Wenli Du

IEEE Access
Multidisciplinary | Rapid Review | Open Access Journal

Received July 8, 2020, accepted July 27, 2020, date of publication August 4, 2020, date of current version August 14, 2020.

Digital Object Identifier 10.1109/ACCESS.2020.3014255

Autonomous Control Strategy for Microgrid Operating Modes Smooth Transition

YARAN LI[1], (Graduate Student Member, IEEE), LONG FU[1], (Student Member, IEEE), KE MENG[1], (Senior Member, IEEE), ZHAO YANG DONG[1], (Fellow, IEEE), KASHEM MUTTAQI[2], (Senior Member, IEEE), AND WENLI DU[3]

[1]School of Electrical Engineering and Telecommunications, University of New South Wales, Kensington, NSW 2052, Australia
[2]School of Electrical, Computer and Telecommunications Engineering, University of Wollongong, Wollongong, NSW 2552, Australia
[3]School of Information Science and Engineering, East China University of Science and Technology, Shanghai 200237, China

Corresponding author: Yaran Li (yaran.li@unsw.edu.au)

This work was supported in part by the University of New South Wales (UNSW) Digital Grid Futures Institute, and in part by the UNSW Tuition Fee Scholarship.

ABSTRACT Microgrid transition between standalone and grid-connected modes is a promising alternative to provide the grid with increasing flexibility and availability. However, transition smoothness relies heavily on control topologies and corresponding parameters, which thus remains challengeable. Existing microgrid transition strategies have two major deficiencies: 1) Inverter control mode alters subjected to microgrid operating mode, for instance, the inverter in current control will switch to voltage control when microgrid disconnects to the utility grid; 2) Controller parameters are selected based on practice and experience, where a systematic and efficient approach does not exist. Motivated by these limitations, in this paper, an autonomous control strategy is proposed for microgrid smooth state transitions. It is highlighted in the following aspects: 1) The cascaded control strategy enables smooth state transition within a single control structure, which permits controller independent of mode switching; 2) Nonlinear-Simplex based algorithm is interfaced with electromagnetic transient simulations, searching for optimal controller parameters in order to minimize voltage deviation in a chain of microgrid events. The effectiveness of the control framework is validated with simulations in PSCAD/EMTDC and RTDS.

INDEX TERMS Microgrid control, parameter tuning, stability analysis, state transition.

NOMENCLATURE

ACRONYMS

CC-VSI	Current controlled – voltage source inverter
DG	Distributed generator
EMT	Electromagnetic transient
GSI	Grid side inverter
MPPT	Maximum power point tracking
OEM	Original equipment manufacturer
PCC	Point of common coupling
PI	Proportional integral
PLL	Phase locked loop
PR	Proportional resonant
PV	Photovoltaic
PWM	Pulse width modulation
RSC	Rotor side converter
RTDS	Real-time digital simulator
SMIB	Single machine infinite bus
THD	Total harmonic distortion
VC-VSI	Voltage controlled – voltage source inverter

PARAMETERS

R_f, L_f, C_f	Resistance, inductance and capacitor of LC filter
R_c, L_c	Resistance and inductance of an autonomous DG connecting to PCC
R_g, L_g	Equivalent resistance and inductance of the grid

VARIABLES AND MATRIX

$i^i_{\alpha\beta}$	Current flowing out of VSI on $\alpha\beta$-frame
i^i_{dq}	Current flowing out of VSI on dq-frame
i^o_{dq}	Current flowing out of LC filter on dq-frame
$v^i_{\alpha\beta}$	Voltage over capacitor bank on $\alpha\beta$-frame

The associate editor coordinating the review of this manuscript and approving it for publication was Giambattista Gruosso.

$v^t_{\alpha\beta}$	Voltage at inverter terminal on $\alpha\beta$-frame
v^i_{dq}	Voltage over capacitor bank on dq-frame
v^o_{dq}	PCC voltage on dq-frame
v^*_{dq}	Reference voltage variables on dq-frame
v_{edq}	Voltage control error on dq-frame
ω	Measured angular frequency of v^i_{abc}
m_i, n_i	Active and reactive power droop coefficients
ω_0	Nominal angular frequency of microgrid

I. INTRODUCTION

Modern power systems have continued to witness transformation in generation, transmission and distribution. Improving the resilience of electric distribution control infrastructure is an urgent issue, not only to reduce vulnerability to extreme events but also to facilitate the integration of renewable energy. Microgrid, a small-scale network containing a set of distributed generators (DGs) and electrical loads, is an emerging and promising solution [1]–[3].

Microgrids are anticipated to be able to transit seamlessly from grid-attached mode to islanded mode in case of grid events (such as transmission/distribution line fault resulting in line outage) and reconnect once the fault is cleared [4]. Nevertheless, the smoothness of transition between these two operational states is a challenge and calls for advanced control strategies. Various techniques have been dedicated on microgrid transition control. Among the options, most existing transition control methodologies were implemented by changing voltage-controlled voltage source inverters (VC-VSIs) to current-controlled voltage source inverters (CC-VSIs), and vice versa [5]–[8]. The main drawback of this approach is that when fault occurs and the microgrid has to transit to islanded states unintentionally, protection devices (e.g. current transformer, voltage transformer, relay, etc.) need sufficient time to detect the fault, acquire data and broadcast new operational assignments, which leads to a blackhole for the microgrid being uncontrolled [9]. To compensate for deteriorated dynamic performances, some researches elaborated designs to optimally reduce total harmonic distortion (THD) [10], the output error between parallel-aligned controllers [11] and small-disturbance response [12], to name just a few. Nonetheless, these studies have limited scalability and capability to be extended to a unified way of controlling microgrid in different operating scenarios. Alternatively, microgrid control strategy adapting to both grid-attached mode and stand-alone mode has been explored to remain within a single control scheme [13], [14]. Majority controllers in this category adopt complex nonlinear control theory to improve the efficiency, e.g. model predictive control as in [13], which from engineering application perspective leads to implementation challenges. Consequently, to authors' knowledge, there is still a lack of generalized microgrid transition control strategy that is compatible with all possible operation modes.

Aside from control system improvement, controller parameter tuning is another issue that urgently seeks for appropriate solutions. In industrial applications, most original equipment manufacturers (OEMs) select controller parameters from practice and experience in a single machine infinite bus (SMIB) testing. With a blind view of rigorously analytical analysis, these solely tuned controllers are potentially causing interaction problems in the inter-connected area [15]. Numerous researchers have been focused on this and developed some parameter tuning methods [16]–[19]. For example, [16] and [17] contribute in establishing parameter selection theorem from controller robustness, small-signal stability and frequency response points of view. On the other hand, researchers have also explored on integrating advanced mathematical techniques to select parameters. For instance, a particle swarm optimization is implemented in [18] to tune the virtual synchronous generator parameters. In [19], simulation-optimization technique is applied to determine power dispatch among DGs, which takes full consideration of nonlinear dynamics during microgrid islanding transitions but without complexifying the optimization problem. Yet, among the existing literature, microgrid transient process (i.e. state transitions including islanding and reconnecting) has not been rigorously analyzed regarding to the controller parameters.

To address these concerns, an autonomous strategy is proposed for microgrid seamless transition in this paper. It has two essential functionalities: 1) Control System: It is configured as a cascaded structure, with inner current control and outer voltage control. Different controllers are chosen in correspondingly appropriate reference frames for voltage and current control [20]. In addition, reference signals for control variables are generated to coordinate among DGs, restore voltage deviations and synchronize phase to grid before reconnection. 2) Parameter Tuning: An objective function is created, aiming at minimizing voltage deviation over microgrid state transitions, and the algorithm is established with a synthetic framework considering about electro-magnetic characteristics, analytic performance assessment and iterative tuning process. To summarize, contributions of the paper are mainly of two folds:

1) The cascaded control topology and the algorithm to generate a robust set of reference signals are proposed, which enables microgrid state transition within a single control structure and permits controller independent of mode switching.

2) Nonlinear-Simplex based algorithm is interfaced with electromagnetic transient simulations, searching for optimal controller parameters in order to minimize voltage deviations in a chain of microgrid events.

The remainder of this paper is structured as follows: Section II elaborates on the proposed control strategy with the state-space modelling. Followed by that, Section III introduces the tuning algorithm for the controller parameters. Section IV extends the discussion on robust stability of the control system upon various uncertainties that potentially leads to dynamic disturbances. Section V demonstrates the proposed strategy via simulation results in PSCAD/EMTDC. Section VI further validates it in real-time digital

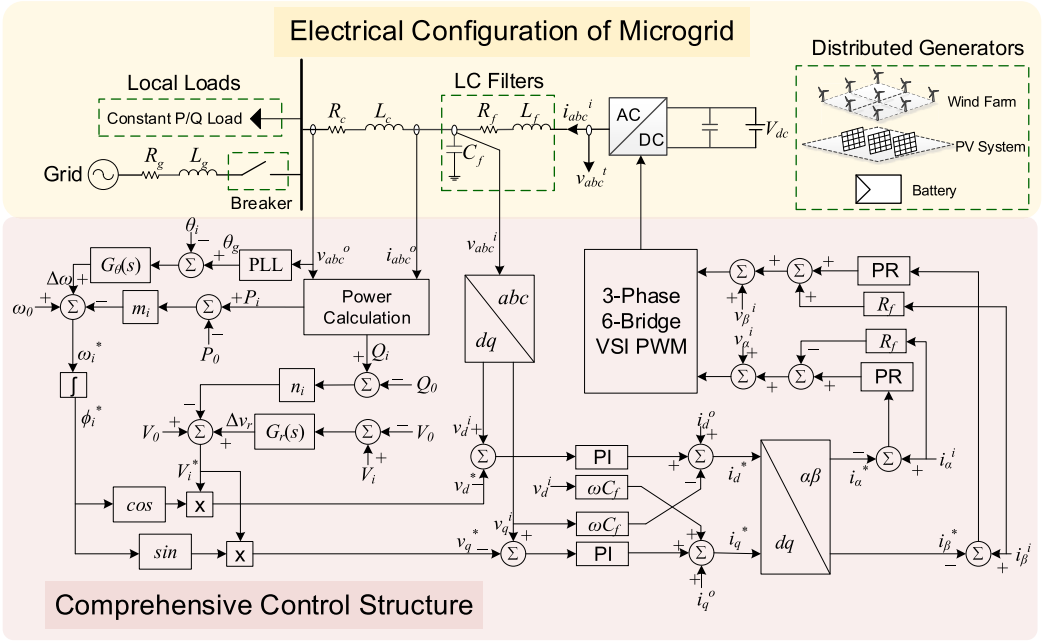

FIGURE 1. Comprehensive control structure with the studied microgrid system.

simulator (RTDS). Section VII discusses assumptions, limitations and future work of this paper. Section VIII draws the conclusion.

II. THE MICROGRID CONTROL STRATEGY

The overall control structure includes: 1) cascaded voltage and current control; 2) centralized voltage restoration and phase synchronization; 3) proportional power dispatch. The comprehensive block diagram of the proposed control strategy, as well as the electrical configuration, is presented in Fig. 1. For the microgrid components, a constant dc-link voltage bus, fed by rotor-side converter of type-4 wind turbines, photovoltaic (PV) arrays and batteries, is assumed, which are integrated to the ac utility grid via pulse width modulation (PWM) controlled voltage source inverters (VSI). To improve the power quality, LC circuit is utilized to filter out harmonics generated from electronic device switching [21]. Besides, line impedances, local loads and the utility grid are considered and commonly connecting PCC. The microgrid is connected or disconnected to the main grid by closing or opening the circuit breaker shown as Fig. 1. The breaker is configured to open following a fault event in the grid, which in turn islands the microgrid. As the proposed control strategy has an integrated single control structure, inverter has no need to transit control modes upon islanding or reconnecting. Therefore, the circuit breaker does not send any signals to the microgrid controller and vice versa.

A. CASCADED VOLTAGE AND CURRENT CONTROL

In this part, firstly, voltage dynamics model is built in dq-synchronously rotating coordination. Based on that, voltage control framework is developed to decouple cross-axis interactions and achieve zero steady-state error. Presumably, current controller having faster dynamics and thus having been stabilized, voltage state-space model shall be constructed for stability analysis. Secondly, current dynamics in $\alpha\beta$-stationary frame, controller principle and state-space model are to be discussed and analyzed. Lastly, we explicitly explain the reasons for conducting voltage and current control in separate frames.

Referring to Fig. 1, voltage dynamics for a single DG entity connecting to the grid can be formulated using the capacitor banks, so that,

$$\begin{cases} \dfrac{dv_d^i}{dt} = \omega v_q^i + \dfrac{1}{C_f} i_d^i - \dfrac{1}{C_f} i_d^o \\ \dfrac{dv_q^i}{dt} = -\omega v_d^i + \dfrac{1}{C_f} i_q^i - \dfrac{1}{C_f} i_q^o. \end{cases} \tag{1}$$

Therefore, to decouple interactions between the quadrature axes, i.e. the terms ωv_q^i and ωv_d^i, voltage control is organized as:

$$i_d^i = k_p^d v_{ed} + \underbrace{k_i^d \int_0^t v_{ed} d\tau}_{\xi_v^d} - \omega C_f v_q^i + i_d^o, \tag{2a}$$

$$i_q^i = k_p^q v_{eq} + \underbrace{k_i^q \int_0^t v_{eq} d\tau}_{\xi_v^q} + \omega C_f v_d^i + i_q^o, \tag{2b}$$

where v_{ed} and v_{eq} are defined as the control error between the reference and the measurement, expressed as:

$$v_{ed} = v_d^i - v_d^* \quad v_{eq} = v_q^i - v_q^*, \tag{3}$$

By implementing (2a) and (2b), voltage PI controllers u_d and u_q enables to track voltage reference with zero steady-state error.

Moreover, the stability of the proposed voltage controller is explored by assessing eigenvalues of the Jacobian matrix of closed loop voltage state-space model. In terms of (1), (2a), (2b) and (3), by defining $x_v = [v_d^i v_q^i]^T$ as the state variables, $u_v = [i_d^i i_q^i]^T$ as the input from the controller, $d_v = [i_d^o i_q^o]^T$ as the disturbance for this state-space model, and $y_v = [v_d^i v_q^i]^T$ as the output, open-loop dynamics for the physical microgrid system is given as:

$$\begin{cases} \dot{x}_v = A_v x_v + B_v u_v + E_v d_v \\ y_v = C_v x_v. \end{cases} \tag{4}$$

where the coefficient matrices are provided in Appendix.

By denoting the integral components in (2a) and (2b) as the state variables of the state space for the open-loop voltage controller $\xi_v = [\xi_v^d \xi_v^q]^T$, the controller dynamics model can be constructed as:

$$\begin{cases} \dot{\xi}_v = A_{Kv}\xi_v + B_{Kv}x_v - B_{Kv}r_v \\ u_v = C_{Kv}\xi_v + D_{Kv}x_v + R_{Kv}r_v + E_{Kv}d_v. \end{cases} \tag{5}$$

Refer to Appendix for the coefficient matrices. Now that combining (4) and (5) obtains the state-space model for closed-loop voltage control in the microgrid, yielding:

$$\begin{cases} \dot{x}_v = (A_v + B_v D_{Kv})\, x_v + B_v C_{Kv}\xi_v \\ \qquad\quad + B_v R_{Kv} r_v + (B_v E_{Kv} + E_v)\, d_v \\ \dot{\xi}_v = B_{Kv}x_v + A_{Kv}\xi_v - B_{Kv}r_v \\ y_v = C_v x_v \end{cases} \tag{6}$$

Accordingly, the Jacobian matrix for the voltage control system is:

$$J_v = \begin{bmatrix} A_v + B_v D_{Kv} & B_v C_{Kv} \\ B_{Kv} & A_{Kv} \end{bmatrix} \tag{7}$$

Current dynamics model in $\alpha\beta$-coordination for the real microgrid plant can be formalized as:

$$\begin{cases} L_f \dfrac{di_\alpha^i}{dt} = -R_f i_\alpha^i + v_\alpha^t - v_\alpha^i \\ L_f \dfrac{di_\beta^i}{dt} = -R_f i_\beta^i + v_\beta^t - v_\beta^i \end{cases} \tag{8}$$

where the voltage and current signals are denoted in Fig. 1. Let us denote $x_c = [i_\alpha^i i_\beta^i]^T$ as the current state variables, $u_c = [v_\alpha^t v_\beta^t]^T$ as the input from the current controller, $d_c = [v_\alpha^i v_\beta^i]^T$ as the disturbance, and $y_c = [i_\alpha^i i_\beta^i]^T$ as the output. The open-loop state-space model for the microgrid plant as for current is:

$$\begin{cases} \dot{x}_c = A_c x_c + B_c u_c + E_c d_c \\ y_c = C_c x_c \end{cases} \tag{9}$$

The coefficient matrices are defined in Appendix.

Adopt PR controller for current control in $\alpha\beta$-frame, which has the equivalence of PI controller in dq-frame in achieving zero steady-state error, such that in s-domain,

$$G_i^{\alpha\beta}(s) = \begin{bmatrix} \cos(\omega t) & -\sin(\omega t) \\ \sin(\omega t) & \cos(\omega t) \end{bmatrix} \begin{bmatrix} G_{PI}(s) & \\ & G_{PI}(s) \end{bmatrix}, \tag{10}$$

where $G_{PI}(s)$ is in a general form of PI controller, that is:

$$G_{PI}(s) = k_p^{\alpha\beta} + \frac{k_i^{\alpha\beta}}{s}. \tag{11}$$

Substitute (11) into (10) and then follow Euler's formula, yielding:

$$G_i^{\alpha\beta}(s) = \frac{1}{2}\begin{bmatrix} G_{PI}^p(s) + G_{PI}^n(s) & jG_{PI}^p(s) - jG_{PI}^n(s) \\ -jG_{PI}^p(s) + jG_{PI}^n(s) & G_{PI}^p(s) + G_{PI}^n(s) \end{bmatrix} \tag{12}$$

where,

$$G_{PI}^p(s) = G_{PI}(s)e^{j\omega t} = G_{PI}(s + j\omega) = k_p^{\alpha\beta} + \frac{k_i^{\alpha\beta}}{s + j\omega}, \tag{13a}$$

$$G_{PI}^n(s) = G_{PI}(s)e^{-j\omega t} = G_{PI}(s - j\omega) = k_p^{\alpha\beta} + \frac{k_i^{\alpha\beta}}{s - j\omega}. \tag{13b}$$

According to (12), the transfer function matrix for the current controller is derived as:

$$G_i^{\alpha\beta}(s) = \begin{bmatrix} k_p^{\alpha\beta} + \dfrac{k_i^{\alpha\beta} s}{s^2 + \omega^2} & -\dfrac{k_i^{\alpha\beta}\omega}{s^2 + \omega^2} \\ \dfrac{k_i^{\alpha\beta}\omega}{s^2 + \omega^2} & k_p^{\alpha\beta} + \dfrac{k_i^{\alpha\beta} s}{s^2 + \omega^2} \end{bmatrix} \tag{14}$$

Converting (14) into time-domain and considering its implementation in the real plant as of (8) obtain:

$$v_\alpha^t = k_p^\alpha i_{e\alpha} + k_i^\alpha \underbrace{\left(\cos(\omega t) i_{e\alpha} - \sin(\omega t) i_{e\beta}\right)}_{\xi_c^\alpha} - R_f i_\alpha^i + v_\alpha^i \tag{15a}$$

$$v_\beta^t = k_p^\beta i_{e\beta} + k_i^\beta \underbrace{\left(\cos(\omega t) i_{e\beta} + \sin(\omega t) i_{e\alpha}\right)}_{\xi_c^\beta} + R_f i_\beta^i + v_\beta^i \tag{15b}$$

where $i_{e\alpha}$ and $i_{e\beta}$ are the current control errors, written as:

$$i_{e\alpha} = i_\alpha^i - i_\alpha^* \quad i_{e\beta} = i_\beta^i - i_\beta^*. \tag{16}$$

Note that for control errors on α-axis and β-axis, respectively, we have,

$$\left\langle \vec{i}_{e\alpha},\ \vec{i}_{e\beta} \right\rangle = 0. \tag{17}$$

Incorporating (15a) and (15b), the state-space model for the current controller dynamics can be derived:

$$\begin{cases} \dot{\xi}_c = A_{Kc}\xi_c + B_{Kc}x_c - B_{Kc}r_c \\ u_c = C_{Kc}\xi_c + D_{Kc}x_c + R_{Kc}r_c + E_{Kc}d_c, \end{cases} \tag{18}$$

where $\xi_c = [\xi_c^d \xi_c^q]^T$ is the state variable vector, and $r_c = [i_\alpha^* i_\beta^*]^T$ is the reference input to the control model, the coefficient matrices are shown in Appendix. Similar to voltage Jacobian matrix, the current Jacobian matrix is:

$$J_c = \begin{bmatrix} A_c + B_c D_{Kc} & B_c C_{Kc} \\ B_{Kc} & A_{Kc} \end{bmatrix} \tag{19}$$

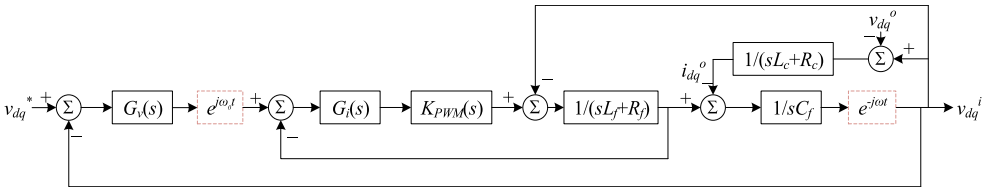

FIGURE 2. Block diagram of the comprehensive control algorithm.

The conclusive schematic for the cascaded voltage and current control synthesis is depicted in Fig. 2, which we would discuss in three parts, i.e. outer voltage loop, inner current loop and plant effects. The inverse Park Transformation is carried out for current reference signals, resulting in voltage control and current control under different reference frames. The consequence of this also involves inserting a block into the overall diagram, highlighting in Fig. 2 with dashed line. The principal motivation of implementing this is driven by application in controlling the microgrid during state transitions, in which period frequency is likely to witness large deviations compared to nominal frequency (e.g. 50Hz in Australia). Under this circumstance, we shall rigorously analyze the following hypotheses: A. Suppose voltage and current control are in dq-frame with PI controllers. B. Suppose voltage and current control in $\alpha\beta$-frame with PR controllers. C. The strategy proposed in this section. For simplicity, we assume a three-phase balanced system that can therefore be equivalent to a single-phase system.

Consider inner current loop combined with plant dynamics first. The input/output transfer function of this aggregation can be developed as:

$$H_{cp}(s) = \frac{G_i(s)K_{PWM}(s)}{C_f L_f s^2 + \left(R_f + G_i(s)K_{PWM}(s)\right) C_f s + 1}. \tag{20}$$

where, $K_{PWM}(s)$ is the gain provided by PWM, and $G_i(s)$ could be either PI controller as in hypothesis A or PR controller as in hypothesis B and C. Next, the outer voltage loop is included to consider the overall input/output transfer function. If there is only a single reference frame, i.e. for hypothesis A and B, the transfer function is:

$$H_{tr}^{ab}(s) = \frac{v_{dq}^i}{v_{dq}^*} = \frac{G_v(s)H_{cp}(s)}{1 + G_v(s)H_{cp}(s)}. \tag{21}$$

Considering using a reference frequency ω_0 to facilitate the inverse Park Transformation, the transfer function for the proposed strategy can be constructed as:

$$H_{tr}^{c}(s) = \frac{v_{dq}^i}{v_{dq}^*} = \frac{G_v(s)H_{cp}(s)}{1 + G_v(s)H_{cp}(s)} e^{j(\omega_0-\omega)t}. \tag{22}$$

From the controller perspective, PI control in the dq-reference frame has been proved to be equivalent to PR control in the $\alpha\beta$-reference frame if they are implemented appropriately and controller parameters are identical [22]. Compared (22) to (21), control topology C has an additional pole regarding frequency deviations, which increases the system type by one that ultimately improves steady-state error. As a result, it should be addressed that this topology design provides superiority particularly for the microgrid that is required to transit from grid-attached state to islanded state and vice versa.

B. REFERENCE GENERATION

The robust reference generation algorithm, including voltage magnitude and phase, is introduced in this part, which accommodates the single structure of the control strategy and avoids switching of reference sets upon microgrid state transition.

Voltage magnitude reference basically comprises of Q-V droop and voltage restoration, formulating as:

$$V_i^* = V_0 - n_i(Q_i - Q_0) + \Delta v_r, \tag{23}$$

where V_i^* is the voltage magnitude reference for the i-th DG, V_0, Q_0 are the nominal voltage and reactive power specified by the generator manufacturer, n_i is the droop coefficient depending on the generator's reactive power capability, Q_i is the measured output reactive power, and Δv_r represents the voltage correction term given by the voltage restoration control:

$$\Delta v_r = \underbrace{(k_p^r + k_i^r/s)}_{G_r(s)}(V_i - V_0), \tag{24}$$

where V_i represents is the measured voltage magnitude at the point of capacitor bank.

Additionally, phase reference is produced by the combination of P-f droop and phase deviation mitigation, given as:

$$\phi_i^* = \int_0^{2\pi} (\omega_0 - m_i(P_i - P_0) + \Delta\omega)d\tau, \tag{25}$$

where ϕ_i^* is the phase reference for the i-th DG, ω_0 and P_0 are the nominal frequency and active power rating for the generator operation, m_i is the droop coefficient depending on the frequency regulation capability, P_i is the measured output active power, and $\Delta\omega$ is controlled by phase synchronization algorithm given by:

$$\Delta\omega = \underbrace{(k_p^\theta + k_i^\theta/s)}_{G_\theta(s)}(\theta_g - \theta_i), \tag{26}$$

where θ_g is the grid phase derived from phase locked loop (PLL), and θ_i is the measured phase at the inverter terminal. This phase synchronization algorithm is based on

a standard PLL to extract the grid phase, with a phase correction term integrated to gradually compensate the phase deviation, especially during microgrid reconnecting to the main grid. Failure to achieve synchronization results in circulating current among the inverters, and in the worst-case triggers resonant oscillations [23], [24].

Coordinating parallelly aligned-DGs, droop coefficients are chosen in order to proportionally dispatch active power and reactive power, so that:

$$\begin{aligned} m_1 P_0^1 = \cdots = m_i P_0^i = \cdots = m_s P_0^s \\ n_1 Q_0^1 = \cdots = n_i Q_0^i = \cdots = n_s Q_0^s, \end{aligned} \tag{27}$$

III. PARAMETER TUNING

This section firstly investigates on the closed-loop response of the overall control strategy. Then an objective function is constructed, reflecting the relationship between microgrid transition performance and controller parameters. Further, optimization algorithm is implemented to tune the corresponding parameters.

A. COMPREHENSIVE CONTROL MODELLING

Fig. 1 depicts the block diagram of the comprehensive control adopted in this paper. Recall transfer functions shown in (14), (20) and (23)-(26), also clarify transfer matrices that represent the proposed control strategy:

$$G_v^{dq}(s) = \begin{bmatrix} k_p^d + k_i^d/s & \\ & k_p^q + k_i^q/s \end{bmatrix} \tag{28}$$

$$H_{cp}^{\alpha\beta}(s) = \frac{G_i^{\alpha\beta}(s) K_{PWM}(s)}{C_f L_f s^2 I^m + \left(R_f I^m + G_i^{\alpha\beta}(s) K_{PWM}(s)\right) C_f s + I^m} \tag{29}$$

where, I^m is the unitary diagonal matrix of two dimensions. Accordingly, the overall output transfer function yields:

$$\begin{aligned} v_{dq}^i = \begin{bmatrix} v_d^i \\ v_q^i \end{bmatrix} = \frac{G_v^{dq}(s) H_{cp}^{\alpha\beta}(s + j\omega_0) e^{JG_\theta(s)(\theta_g - \theta_i)/s}}{I^m + G_v^{dq}(s) H_{cp}^{\alpha\beta}(s + j\omega_0)} \\ \cdot \left((1 - G_r(s)) \begin{bmatrix} V_0 \cos\phi_0 \\ V_0 \sin\phi_0 \end{bmatrix} + G_r(s) \begin{bmatrix} V_i \cos\phi_0 \\ V_i \sin\phi_0 \end{bmatrix} \right), \end{aligned} \tag{30}$$

where we denote,

$$J = \begin{bmatrix} 0 & -1 \\ 1 & 0 \end{bmatrix}. \tag{31}$$

B. PARAMETER TUNING ALGORITHM

An optimization algorithm that interfaces with the electromagnetic simulation is introduced to tune controller parameters and LC filter values towards minimum voltage deviation. Recall the parameters are associated transfer matrices, the variables and constants are to be reversed, which means:

$$G_v^{dq}(s) \rightarrow G_v^{dq}(k_p^d, k_i^d, k_p^q, k_i^q) \tag{32a}$$

$$G_i^{\alpha\beta}(s) \rightarrow G_i^{\alpha\beta}(k_p^{\alpha\beta}, k_i^{\alpha\beta}) \tag{32b}$$

$$G_r(s) \rightarrow G_r(k_p^r, k_i^r) \tag{32c}$$

$$G_\theta(s) \rightarrow G_\theta(k_p^\theta, k_i^\theta) \tag{32d}$$

$$H_{cp}^{\alpha\beta}(s) \rightarrow H_{cp}^{\alpha\beta}(L_f, C_f) \tag{32e}$$

The objective function as in (33) is formulated based on integral square error over the period of microgrid state transitions, which assesses and minimizes the voltage deviations in a compressed Euclidean form.

$$\min_{K_p, K_i, \Omega_f \in \mathbb{R}} \sum_{i=1}^{n} \frac{1}{s} \left(\left\| v_{dq}^i \right\|_2 - \left\| v_0^{dq} \right\|_2 \right)^2 \tag{33}$$

$$s.t.\ \forall K_p \geq 0 \tag{34a}$$

$$\forall\ K_i \geq 0 \tag{34b}$$

$$\forall\ \Omega_f > 0 \tag{34c}$$

where $v_0^{dq} = [V_0 cos\phi_0\ V_0 sin\phi_0]^T$, $K_p = \{k_p^d, k_p^q, k_p^{\alpha\beta}, k_p^r, k_p^\theta\}$, $K_i = \{k_i^d, k_i^q, k_i^{\alpha\beta}, k_i^r, k_i^\theta\}$, and $\Omega_f = \{L_f, C_f\}$. Consequently, the objective function (33) is a function of controller parameters.

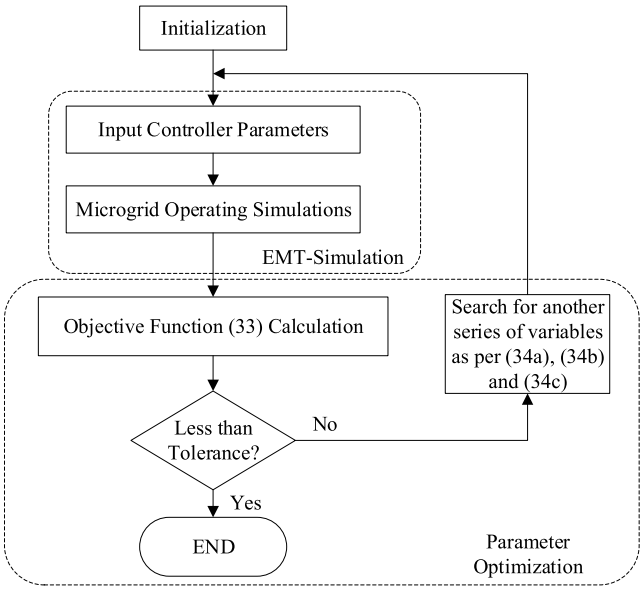

FIGURE 3. Flow diagram of parameter tuning algorithm.

The objective (33) is a function with significantly high nonlinearities and high-order derivatives. Nonlinear-Simplex algorithm is a geophysical evolution in a multi-dimensional space for multi-objective optimization to converge to the feasible solutions [25]. This optimization methodology has a fast converging speed as the worst case of vertex will be replaced by the centroid of the rest vertices, with the searching area being expanded or contracted. Also, nonlinear-Simplex algorithm is a type of optimization free of derivatives, which provides computational opportunities to interface electromagnetic transient (EMT) simulations with optimization algorithm [26]. Hence, the nonlinear-Simplex method is utilized in this paper to solve the problem (33)-(34). Fig. 3 clarifies simulation-interfaced optimization process for the parameter tuning algorithm.

Furthermore, the procedure of the parameter tuning algorithm is outlined as follows:

Step 1 (Initialization): Enter a set of initial controller parameters and LC filter values that are compliant with the constraints in (34a), (34b) and (34c).

Step 2 (EMT-Simulations): Simulate microgrid with a chain of events, i.e. black start with the grid connected, then disconnect the grid to island the microgrid, and also reconnect.

Step 3 (Parameter Optimization): Assess the microgrid performance during the simulations by collecting voltage data from step 2 and calculating the objective function as (33). If that does not satisfy the pre-set tolerance, search for another set of variables that are within the ranges of (34a), (34b) and (34c), and exit the process until the tolerance is satisfied.

IV. ROBUSTNESS ANALYSIS

The robust stability of the proposed control system shall be evaluated in three aspects in this section.

A. VOLTAGE CONTROL SYSTEM

Reference tracking performance and system performance of the voltage control system are analyzed, with the voltage reference and load uncertainties as the major disturbances that lead to voltage dynamic disturbances. This is mainly focused on the microgrid islanding operation.

For the reference tracking in the cascaded voltage-current control system, define the tracking error as the performance output and the reference input as the disturbance. The transfer function from the voltage reference to the tracking error is obtained as in the following:

$$S_{ve}(s) = \frac{1}{1 + G_v(s)H_{cp}(s)}, \tag{35}$$

where $G_v(s)$ is the voltage controller and $H_{cp}(s)$ is the input/output transfer function of the inner current loop combined with the plant dynamics. Then we discuss the boundary of the disturbance (voltage reference), which is the drifting from the nominal voltage as a result of droop control. Estimate the upper bound of the frequency characteristic of the disturbance for voltage reference and denote as $W_{vt}(s)$. This transfer function is chosen such that: 1) the peak of the frequency response is at 50Hz; 2) it can accommodate the frequency deviations and provide sufficient bandwidth to cover the response of droop controller. Therefore, the following form is utilized for $W_{vt}(s)$ to justify robustness of the closed-loop control system regarding reference tracking:

$$W_{vt}(s) = \frac{\omega_{vt}^2}{s^2 + 2\varsigma_{vt}\omega_{vt}s + \omega_{vt}^2}, \tag{36}$$

where ω_{vt} is the line frequency, i.e. $2\pi \cdot 50$rad/s, and ς_{vt} is the damping ratio that can be varied to adjust the resonant peak and control bandwidth. In this case, we select the damping ratio $\varsigma_{vt} = 0.4$.

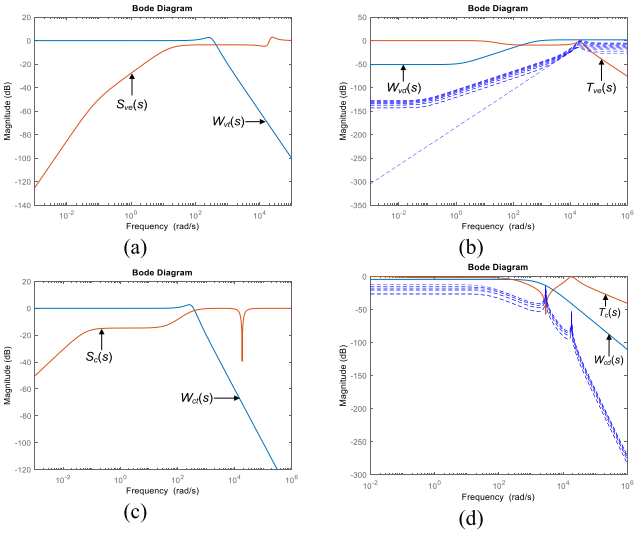

FIGURE 4. Frequency characteristics of corresponding transfer functions.

Considering (35) and (36), the robust stability with respect to reference disturbance can be assured if:

$$\|S_{ve}W_{vt}\|_\infty < 1. \tag{37}$$

According to the controller parameters acquired from the optimization algorithm, Fig. 4(a) presents the frequency response of sensitivity function $S_{ve}(s)$ and its corresponding weighting function $W_{vt}(s)$.

In addition, system uncertainties, specifically uncertainties in filter parameter, L_f and C_f, are analyzed as the major disturbance that potentially leads to voltage dynamic uncertainty. According to the controller topology, the plant set is modelled with multiplicative uncertainty to incorporate parameter uncertainty, so that:

$$\tilde{H}_{cp}(s) = (1 + \Delta W_{vd})H_{cp} \, \|\Delta\|_\infty \le 1, \tag{38}$$

where $\Delta(s)$ is the normalized uncertainty, and $W_{vd}(s)$ is the weighting function that bounds the uncertainty set. In terms of (38), it can be derived that $W_{vd}(s)$ needs to satisfy:

$$|W_{vd}(s)| \ge \left| \frac{\tilde{H}_{cp}}{H_{cp}} - 1 \right|. \tag{39}$$

Considering the system parameters L_f and C_f of $\pm 20\%$ variations around the values obtained from the parameter tuning algorithm, magnitude of RHS (right-hand side) transfer function can be illustrated in bode plot in Fig. 4(b). Accordingly, $W_{vd}(s)$ is chosen such that its magnitude is larger than the clustering uncertainty curves at any frequencies, denoted as:

$$W_{vd}(s) = \frac{7(0.64s + 1)}{200(0.0015s + 1)}. \tag{40}$$

Then, we conduct an equivalent transformation of closed-loop system with uncertainty to separate the uncertainty Δ from the complementary plant, denoting as $M_v(s)$, and apply

the small-gain theorem to ensure the robust stability of the system with respect to load uncertainties:

$$\|M_v(s)\|_\infty = \left\| \frac{W_{vd} G_v H_{cp}}{1 + G_v H_{cp}} \right\|_\infty < 1. \quad (41)$$

Fig. 4(b) exhibits the frequency response of the complementary sensitivity function $T_{ve}(s)$, i.e.:

$$T_{ve}(s) = \frac{G_v(s) H_{cp}(s)}{1 + G_v(s) H_{cp}(s)}. \quad (42)$$

B. CURRENT CONTROL SYSTEM

This section mainly investigates robustness of current control during grid-attached operation. The current closed-loop system consists of the current controller, LC filter and line impedances, interpreting the block diagram as in Fig. 2.

To evaluate the reference tracking performance, current tracking error and the reference input are treated as the performance output and input, respectively. Hence, the transfer function can be obtained as:

$$S_c(s) = \frac{1}{1 + G_i(s) K_{PWM}(s) H_{fg}(s)}, \quad (43)$$

where $S_c(s)$ is denoted as the sensitivity function of the system, and $H_{fg}(s)$ consists of plant effects from LC filter, and connecting line impedances, formulated as:

$$H_{fg}(s) = \frac{L_c C_f s^2 + R_c C_f s + 1}{(L_f s + R_f)\left(L_c C_f s^2 + R_c C_f s + 1\right) + L_c s + R_c}. \quad (44)$$

Additionally, the weighting function $W_{ct}(s)$ is selected to shape the frequency response characteristics of the transfer function $S_c(s)$, ensuring high gain at the line frequency and low gain at the harmonics, so chosen as:

$$W_{ct}(s) = \frac{\omega_{ct}^2}{s^2 + 2\varsigma_{ct}\omega_{ct} s + \omega_{ct}^2}, \quad (45)$$

where ω_{ct} is the line frequency, and ς_{ct} is the damping ratio that can provide the freedom to adjust the resonant peak and the bandwidth. Given the controller parameters and system conditions, line frequency ω_{ct} is $2\pi \cdot 50$rad/s, ς_{vt} has been selected as 0.4.

For the robust performance with respect to system parameter variations (e.g. L_c, and R_c), we model the plant set with multiplicative uncertainties [27], such that:

$$\tilde{H}_{fg}(s) = (1 + \Delta W_{cd})\, H_{fg} \; \|\Delta\|_\infty \le 1, \quad (46)$$

where $\Delta(s)$ is the normalized disturbance, and $W_{cd}(s)$ is the weighting function that is reformulated to reflect the upper bound of the disturbance:

$$|W_{cd}(s)| \ge \left| \frac{\tilde{H}_{fg} - H_{fg}}{H_{fg}} \right|. \quad (47)$$

As depicted in Fig. 4(c), the magnitude of the selected weighting function is larger than the clustering curves of RHS of (47) with ±20% of system parameter perturbations.

The transfer function of the weighting function can be expressed as:

$$W_{cd}(s) = \frac{0.598}{2 \times 10^{-7} s^2 + 10^{-3} s + 1}. \quad (48)$$

The following mixed-sensitivity criterion is adopted to comprehensively assess the robust stability of the system:

$$\left\| \begin{matrix} W_{ct} S_c \\ W_{cd} T_c \end{matrix} \right\|_\infty < 1, \quad (49)$$

where $T_c(s)$ is the complementary sensitivity of the system that satisfies:

$$T_c(s) = 1 - S_c(s) = \frac{G_i(s) K_{PWM}(s) H_{fg}(s)}{1 + G_i(s) K_{PWM}(s) H_{fg}(s)}. \quad (50)$$

C. STRUCTURAL ROBUSTNESS

The proposed microgrid control strategy has the cascaded topology that enables microgrid grid-connected operation and islanded operation within a single control structure, which thus eliminates the switching disturbances during mode transfer. Hence, the control strategy is of remarkable structural robustness.

V. RESULTS AND ANALYSIS

The simulations validate the proposed control strategy in three aspects: 1) smooth and seamless transitions between grid-connected state and islanded state; 2) equal power sharing among DGs; 3) minimum voltage deviation and harmonic distortion in voltage and current. A microgrid displayed in Fig. 5 has been built up in PSCAD/EMTDC and RTDS, which electrically consists of three parallelly aligned DG units that are modelled as ideal dc voltage sources, two constant active and reactive power loads, and the main grid. This section would demonstrate simulations with a chain of microgrid events. System details are listed in Table 1.

TABLE 1. System details and controller parameters.

Symbol	Description	Value
V_{dc}	DC link voltage	650V
V_{grid}	Grid voltage level	230V
ω_0	Nominal frequency	314.1593rad/s
f_{sw}	Switching frequency	8kHz
m, n	Droop coefficients	0.1Hz/MW, 0.1kV/MVar
P_l, Q_l	Constant P/Q loads	0.3MW, 0.3MVar
P_0, Q_0	Nominal ratings of DGs	0.2MW, 0.2MVar

Also, the proposed control scheme with optimal parameters (hereafter "Proposed Control") is compared to the existing control strategy as in [5]–[8] (hereafter "Conventional Control") and the proposed control scheme with initialized parameters (hereafter "Initialized Parameters"). The conventional control strategy generally has voltage control mode for microgrid islanded operation and current control mode for grid-attached operation, and controller shall switch the mode when microgrid state transits correspondingly. Details about the most existing control strategies are provided in the Appendix.

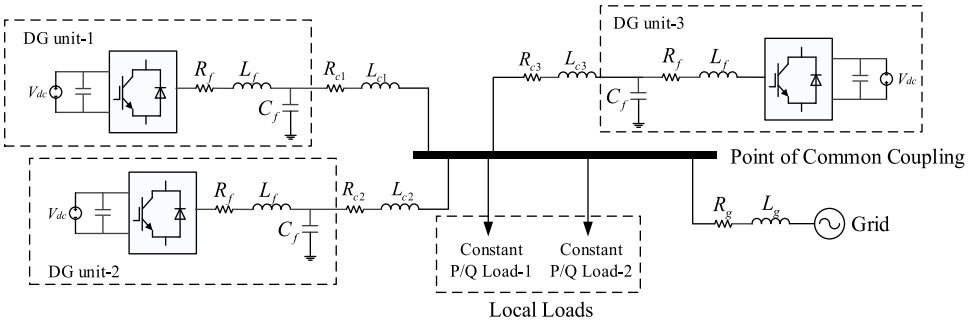

FIGURE 5. Topology of the studied microgrid system.

The following contents are mainly of two aspects:

1) The process and outcome for the proposed parameter tuning algorithm: Part A;

2) Comparative simulations towards microgrid operating mode transition from grid-tied operation to stand-alone operation, and vice versa: Part B, Part C and Part D;

TABLE 2. Initialization and optimization values for controller parameters.

Variables	Initial Value	Optimized Value
Controller		
$k_p{}^d$	1	71.0064
$k_i{}^d$	1	21.775
$k_p{}^q$	1	5.4334
$k_i{}^q$	1	26.2965
$k_p{}^{\alpha\beta}$	1	0.9278
$k_i{}^{\alpha\beta}$	1	0.0697
$k_p{}^r$	1	21.1795
$k_i{}^r$	1	0.1588
$k_p{}^\theta$	1	15.9698
$k_i{}^\theta$	1	3.2945
LC Filter		
L_f	1H	0.19mH
C_f	20μF	24μF

A. OPTIMIZATION PROCESS FOR TUNING ALGORITHM

The initialized and the optimized results for controller parameters and LC filter values have been listed in Table 2. The optimization algorithm halts at its 119th run, with objective function converging to 0.0092. As indicated in Fig. 6-8 that illustrate microgrid performances in details, the optimal controller parameters from the proposed tuning algorithm can give rise to superior microgrid performances subject to state transitions, with the steady state operation also assured.

In terms of coefficient matrix J_v and J_c, eigenvalues for voltage and current closed-loop system can be provided as: -11443000, -612630, -0.3392 and -7.1573 for voltage control system, -6906.4, -0.35781 ± 314.18i for current control system. All of them are located at left-pane of imaginary axis, which theoretically validates the stability of the control scheme. Furthermore, voltage and current robustness indicators as in (37), (41) and (49) hold.

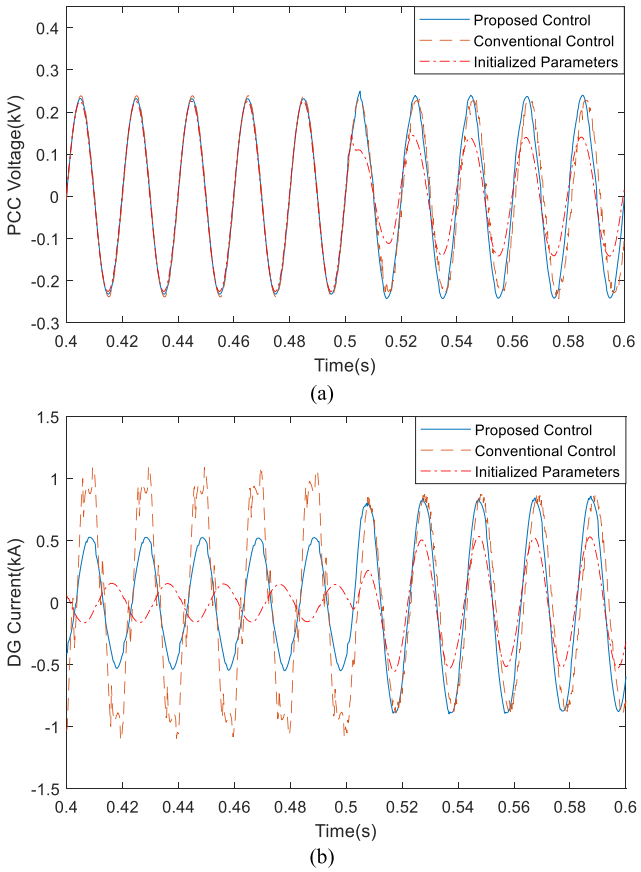

FIGURE 6. Microgrid performances in transition from grid-connected state to islanded state. (a) PCC voltage. (b) DG current.

B. ISLANDING EVENT

The simulation is initialised with the main grid connected, The utility grid is disconnected to the microgrid at t = 0.5s, after which microgrid would be displaced with islanded state.

As shown in Fig. 6(a), PCC voltage magnitudes controlled by all methodologies could track that of the utility grid accurately, with full compensation for loads. However, when islanding is triggered, voltage magnitude and phase

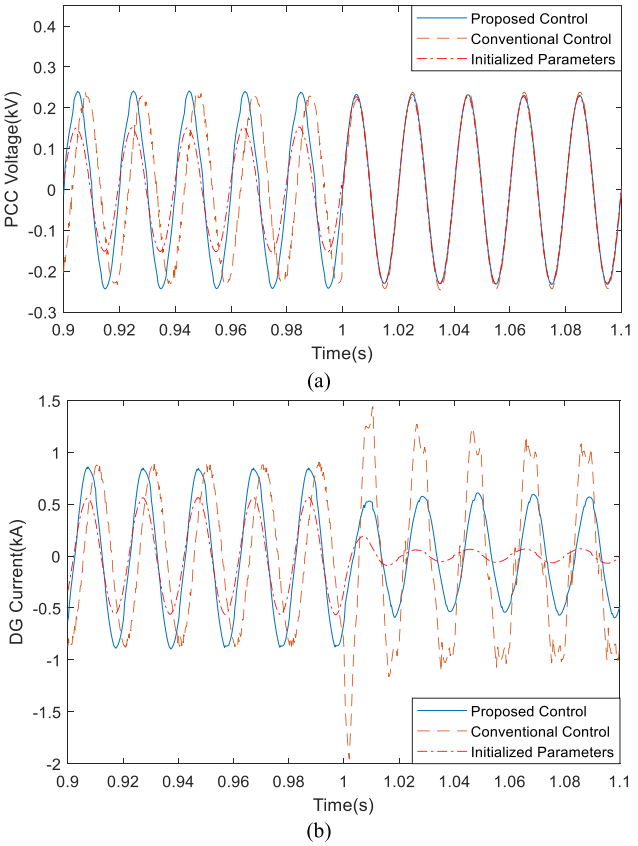

FIGURE 7. Microgrid performances for reconnection from islanded state to grid-connected state. (a) PCC voltage. (b) DG current.

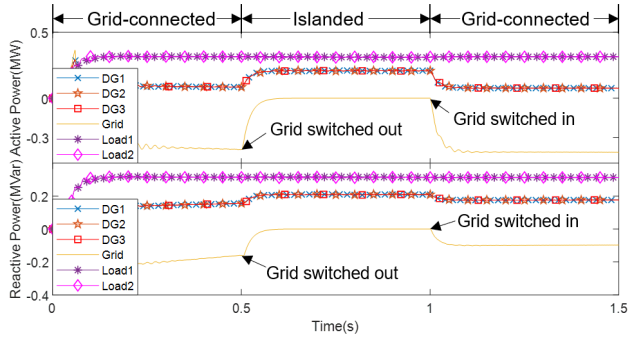

FIGURE 8. Active and reactive power sharing among DGs.

behave differently under different control schemes. Under the proposed control strategy with optimized parameters, the voltage magnitude of microgrid would be violated away from 0.23kV to 0.246kV, and it will quickly restore to the nominal voltage magnitude. Nonetheless, the microgrid PCC voltage controlled by the conventional control strategy has a phase mismatch in stand-alone operation, and a dramatical magnitude drop is observed respect to the proposed control strategy with initialized parameters.

According to the Fig. 6(b), DG output current in the proposed control strategy is capable of smoothly adjusting output current to fully compensate the local loads. While for the conventional control strategy, it has large current distortion in grid-connected states and phase jump upon state transitions. For the initialized parameters, an undesirable phase transient is encountered at the instant of the islanding event.

C. RECONNECTION EVENT

The microgrid is set to be reconnected to the utility grid at t = 1s. The voltage and current performances during the reconnection event are given in Fig. 7(a) and Fig. 7(b), respectively. The proposed control strategy can remain voltage magnitude at 0.23kV after reconnection, which is a key indicator that microgrid succeeds in reconnecting to the utility grid. In addition, PCC voltage phase can be rapidly synchronized with that of the utility grid. Comparably, PCC voltage magnitude with initialized parameters decreases to 0.15kV during islanded states. Moreover, the PCC voltage under the conventional control strategy has phase difference, which results in large disturbances during reconnection process and needs longer time to settle down.

As for DG output current shown in Fig. 7(b), the conventional control strategy fails to seamlessly respond to state transitions, since it witnessed an inrush current with severe harmonic distortion. For the proposed control strategy with optimized controller parameters, DG output current has a satisfied response with small harmonic distortion and phase synchronization.

D. COMPREHENSIVE ASSESSMENT OF MICROGRID

In terms of RMS voltage deviations and frequency fluctuation, an index is proposed to justify the seamless transition of the microgrid operation:

$$f_{st} = \frac{\Delta V_{rms}}{V_{rms,nom}} + \frac{\Delta f}{f_{nom}} + \text{THD} \tag{51}$$

where, ΔV_{rms} and Δf represent maximum PCC RMS voltage deviations and frequency fluctuation during microgrid state transition event. $V_{rms,nom}$ and f_{nom} are nominal RMS line voltage and frequency, respectively, and voltage THD is extracted for the whole period of state transition. The state transition characteristics under the three control strategies are displayed as in Table 3 and Table 4.

TABLE 3. Assessment for islanding event.

	ΔV_{rms}(kV)	Δf(Hz)	THD(%)	f_{st}(%)
Proposed Control	**0.0011**	**0.13**	**2.54**	**3.19**
Conventional Control	0.0103	0.95	2.98	8.53
Initialized Parameters	0.1148	1.19	30.99	74.08

As indicated from Table 3 and 4, the proposed control strategy has achieved smooth state transitions for microgrid. Even though it is marginally better than the conventional control for islanding, the salient merit is found during microgrid reconnection to the grid. Fig. 8 illustrates real and reactive power sharing of the microgrid system in the entire chain of events. Each load has the request of 0.3MW active power

TABLE 4. Assessment for reconnection event.

	ΔV_{rms}(kV)	Δf(Hz)	THD(%)	f_{st}(%)
Proposed Control	**0.0017**	**0.20**	**2.66**	**3.66**
Conventional Control	0.0121	0.67	55.71	61.34
Initialized Parameters	0.0959	0.35	11.25	45.96

and 0.3MVar reactive power, respectively. During the grid-connected state, the utility grid and DGs simultaneously provide power for the local load, with the stiff utility grid absorbing abundant portions. DGs can equally share active power and reactive power as per regulated of their identical capabilities. When it is lack of support from the mains as in stand-alone operation, each DG contributes 0.2MW and 0.2MVar to the microgrid, which could exactly feed two loads each with 0.3MW active power and 0.3MVar reactive power.

VI. REAL-TIME VALIDATION

To validate that the proposed control strategy is also compatible with practical applications, the microgrid is modelled in RTDS. Fig. 9 illustrates the microgrid performances in aspects of PCC voltage, DG output current and power sharing. Overall, the results from RTDS have substantial similarities to the simulation results. However, as control delays and nonideal devices coexist in the microgrid operation, PCC voltage will take longer time to achieve the steady state, and power dissipation slightly defers from simulation results.

More specifically, PCC voltage drops from 0.23kV to 0.2kV when islanding event happens. Nevertheless, it will eventually restore to the nominal rating as indicated in Fig. 9(c). Compared to seamless phase shift upon reconnection as in Fig. 7(a), PCC voltage will experience a phase shift to synchronize to the utility grid. It is due to control delays in real application system. Another difference is that the utility grid barely contributes to the active power sharing. This phenomenon is due to that circuit components, such as breakers, also consume active power, which has been more accurately reflected in RTDS modelling and implementation. However, from system coordination perspective, the local load demand can be compensated in microgrid operation, and power is equally shared among DGs. Thus, active power sharing is acceptable to be different from simulations.

VII. DISCUSSIONS

In this section, the assumptions involved in the case studies, limitations of the proposed control strategy and further work are to be discussed.

Assumption 1: The dc link voltage is considered stiff in the study. An autonomous control strategy for microgrid operating modes smooth transition has been proposed in this paper, which is dedicated on grid side inverter control design. Consequently, the renewable energy sourced distributed generators are modelled as ideal dc voltage sources in the studies.

As shown in Fig. 10, PV modules, interconnecting to battery storage system, are connected to the grid with dc/dc

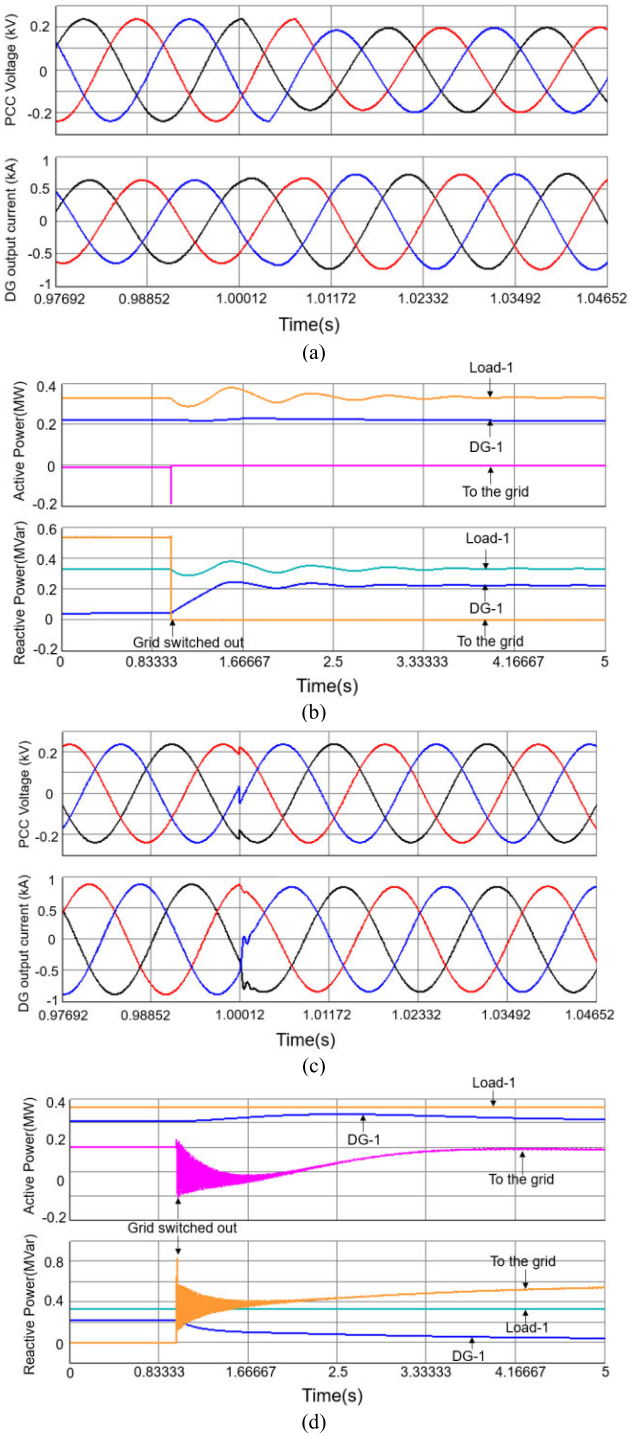

FIGURE 9. Microgrid performances in RTDS. (a) PCC voltage and DG output current during islanding event. (b) Active and reactive power during islanding event. (c) PCC voltage and DG output current during reconnection. (d) Active and reactive power during reconnection event.

inverters and dc/ac inverters in the most current renewable connections [28], [29]. For the dc/dc converter control, it is anticipated to achieve the maximum power point tracking (MPPT) and also regulate the output to a pre-defined value. Control techniques to coordinate PV arrays and batteries have been widely investigated and well established in

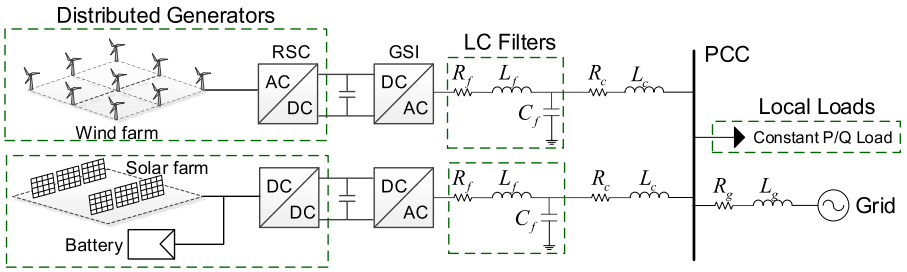

FIGURE 10. An illustration of typical microgrid system layout.

the existing literature, e.g. [30], [31], to minimize the impacts of DG dynamics on the microgrid operation and maintain the dc-bus voltage with less oscillations and overshoots under fluctuating power generation. For the application to integrate wind sources, type-4 wind turbines are connected to the grid with rotor side converter (RSC) and grid side inverter (GSI), from which standard RSC can stabilize dc side voltage [32]. Hence, with appropriate dc-link voltage control, it is reasonable to assume that the dynamic behaviour of DGs is negligible and microgrid state transition control design can be narrowed to dc/ac inverters.

Assumption 2: Uninterruptible communication with the grid is considered in the control strategy. As introduced in Section II Part C, phase synchronization controller at centralized layer mitigates phase deviations for microgrid operation. This control scheme requires the uninterruptible communication between the grid and the inverter controller, even under the circumstance that the grid is electrically isolated from the inverter.

Limitation: The impacts from control delay and communication delay are exclusive from the studies. In other words, delays are nor analytically analysed and accurately modelled in the simulations. Oscillations in active and reactive power are the indicators of the drawback due to this limitation.

Future work: Based on the autonomous control strategy for microgrid operating modes transition proposed in this paper, future work can be dedicated on considering intermittency and uncertainty of renewable energy sourced DGs, which is to address the *Assumption 1*. Also, the impacts from ancillary layers in microgrid can be further investigated, for instance, communication failure and delays. Control delays will be rigorously analysed and accurately modelled in the simulations. Last but not least, experimental test of the proposed control methodology will be conducted in the future work.

VIII. CONCLUSION

A control strategy for microgrid smooth state transition has been presented in this paper. It has been designed to achieve: 1) optimal controller parameters and LC filter values based on voltage deviation; 2) independence of controller conversions towards microgrid state transitions; 3) improvement in voltage stability and phase synchronization of the microgrid under states transition. The proposed control strategy is based on cascaded structure. Furthermore, an objective function is introduced to search for parameters via nonlinear-Simplex algorithm. Under the proposed control strategy, a seamless and robustness state transition could be acquired. Parameter tuning algorithm would significantly contribute to automation of the microgrid.

APPENDIX

A. MATRIX IN VOLTAGE STATE-SPACE MODEL

$$A_v = \begin{bmatrix} 0 & \omega \\ -\omega & 0 \end{bmatrix}, \quad B_v = \frac{1}{C_f} I_{2\times 2}, C_v = I_{2\times 2},$$
$$E_v = -\frac{1}{C_f} I_{2\times 2}, \quad A_{Kv} = 0_{2\times 2}, \quad B_{Kv} = \begin{bmatrix} k_i^d & \\ & k_i^q \end{bmatrix},$$
$$C_{Kv} = I_{2\times 2}, \quad D_{Kv} = \begin{bmatrix} k_p^d & \omega C_f \\ -\omega C_f & k_p^q \end{bmatrix}, \quad R_{Kv} = -I_{2\times 2},$$
$$E_{Kv} = I_{2\times 2}.$$

B. MATRIX IN CURRENT STATE-SPACE MODEL

$$A_c = -\frac{R_f}{L_f} I_{2\times 2}, \quad B_c = \frac{1}{L_f} I_{2\times 2}, \; C_v = I_{2\times 2},$$
$$E_c = -\frac{1}{L_f} I_{2\times 2}, \quad A_{Kc} = \begin{bmatrix} 0 & -\omega \\ \omega & 0 \end{bmatrix}, \quad B_{Kc} = I_{2\times 2},$$
$$C_{Kc} = \begin{bmatrix} k_i^\alpha & \\ & k_i^\beta \end{bmatrix}, \quad D_{Kc} = \begin{bmatrix} k_p^\alpha - R_f & \\ & k_p^\beta + R_f \end{bmatrix},$$
$$R_{Kc} = -\begin{bmatrix} k_p^\alpha & \\ & k_p^\beta \end{bmatrix},$$
$$E_{Kc} = I_{2\times 2}, \quad k_p^\alpha = k_p^\beta = k_p^{\alpha\beta}, \; k_i^\alpha = k_i^\beta = k_i^{\alpha\beta}.$$

C. CONTROLLER PARAMETERS

Most of the existing control approaches [5]–[8] implements the microgrid state transition by switching from CC-VSIs to VC-VSIs, and vice versa. For the comparative simulations in Section IV, the identical microgrid system and DGs are adopted. Moreover, the controllers and corresponding parameters are given as follows. LC filter: $L_f = 0.26$mH, $C_f = 6\mu$F. Voltage PI controller on d-axis: $k_p = 68.6606$, $k_i = 23.31$. Voltage PI controller on q-axis: $k_p = 68.6606$, $k_i = 23.31$. Current PI controller on d-axis: $k_p = 10.69$, $k_i = 0.008$. Current PI controller on q-axis: $k_p = 10.69$, $k_i = 0.008$.

REFERENCES

[1] K. Mahmud, A. K. Sahoo, J. Ravishankar, and Z. Y. Dong, "Coordinated multilayer control for energy management of grid-connected AC microgrids," *IEEE Trans. Ind. Appl.*, vol. 55, no. 6, pp. 7071–7081, Dec. 2019, doi: 10.1109/TIA.2019.2931490.

[2] U. Bose, S. K. Chattopadhyay, C. Chakraborty, and B. Pal, "A novel method of frequency regulation in microgrid," *IEEE Trans. Ind. Appl.*, vol. 55, no. 1, pp. 111–121, Jan. 2019.

[3] Y. Guo, L. Chen, X. Lu, J. Wang, T. Zheng, and S. Mei, "Region-based stability analysis for active dampers in AC microgrids," *IEEE Trans. Ind. Appl.*, vol. 55, no. 6, pp. 7671–7682, Nov. 2019, doi: 10.1109/TIA.2019.2913819.

[4] J. Rocabert, R. Capo-Misut, R. S. Munoz-Aguilar, J. I. Candela, and P. Rodriguez, "Control of energy storage system integrating electrochemical batteries and supercapacitors for grid-connected applications," *IEEE Trans. Ind. Appl.*, vol. 55, no. 2, pp. 1853–1862, Mar./Apr. 2019.

[5] G. M. S. Azevedo, F. Bradaschia, M. C. Cavalcanti, F. A. S. Neves, J. Rocabert, and P. Rodriguez, "Safe transient operation of microgrids based on master-slave configuration," in *Proc. IEEE Energy Convers. Congr. Expo.*, Sep. 2011, pp. 2191–2195.

[6] Y. A.-R.-I. Mohamed, H. H. Zeineldin, M. M. A. Salama, and R. Seethapathy, "Seamless formation and robust control of distributed generation microgrids via direct voltage control and optimized dynamic power sharing," *IEEE Trans. Power Electron.*, vol. 27, no. 3, pp. 1283–1294, Mar. 2012.

[7] M. N. Arafat, A. Elrayyah, and Y. Sozer, "An effective smooth transition control strategy using droop-based synchronization for parallel inverters," *IEEE Trans. Ind. Appl.*, vol. 51, no. 3, pp. 2443–2454, Jun. 2015.

[8] M. Ganjian-Aboukheili, M. Shahabi, Q. Shafiee, and J. M. Guerrero, "Seamless transition of microgrids operation from grid-connected to islanded mode," *IEEE Trans. Smart Grid*, vol. 11, no. 3, pp. 2106–2114, May 2020, doi: 10.1109/TSG.2019.2947651.

[9] J. Xiao, P. Wang, and L. Setyawan, "Implementation of Multiple-Slack-Terminal DC microgrids for smooth transitions between grid-tied and islanded states," *IEEE Trans. Smart Grid*, vol. 7, no. 1, pp. 273–281, Jan. 2016.

[10] M. N. Arafat, S. Palle, Y. Sozer, and I. Husain, "Transition control strategy between standalone and grid-connected operations of voltage-source inverters," *IEEE Trans. Ind. Appl.*, vol. 48, no. 5, pp. 1516–1525, Sep./Oct. 2012.

[11] D. Das, G. Gurrala, and U. J. Shenoy, "Linear quadratic regulator-based bumpless transfer in microgrids," *IEEE Trans. Smart Grid*, vol. 9, no. 1, pp. 416–425, Jan. 2018.

[12] J. Wang, N. C. P. Chang, X. Feng, and A. Monti, "Design of a generalized control algorithm for parallel inverters for smooth microgrid transition operation," *IEEE Trans. Ind. Electron.*, vol. 62, no. 8, pp. 4900–4914, Aug. 2015.

[13] S. Sajadian and R. Ahmadi, "Model predictive control of dual-mode operations Z-source inverter: Islanded and grid-connected," *IEEE Trans. Power Electron.*, vol. 33, no. 5, pp. 4488–4497, May 2018.

[14] G. Lou, W. Gu, J. Wang, J. Wang, and B. Gu, "A unified control scheme based on a disturbance observer for seamless transition operation of inverter-interfaced distributed generation," *IEEE Trans. Smart Grid*, vol. 9, no. 5, pp. 5444–5454, Sep. 2018.

[15] D. G. Holmes, T. A. Lipo, B. P. McGrath, and W. Y. Kong, "Optimized design of stationary frame three phase AC current regulators," *IEEE Trans. Power Electron.*, vol. 24, no. 11, pp. 2417–2426, Nov. 2009.

[16] L. Harnefors, M. Hinkkanen, U. Riaz, F. M. M. Rahman, and L. Zhang, "Robust analytic design of power-synchronization control," *IEEE Trans. Ind. Electron.*, vol. 66, no. 8, pp. 5810–5819, Aug. 2019.

[17] X. Meng, J. Liu, and Z. Liu, "A generalized droop control for grid-supporting inverter based on comparison between traditional droop control and virtual synchronous generator control," *IEEE Trans. Power Electron.*, vol. 34, no. 6, pp. 5416–5438, Jun. 2019.

[18] J. Alipoor, Y. Miura, and T. Ise, "Stability assessment and optimization methods for microgrid with multiple VSG units," *IEEE Trans. Smart Grid*, vol. 9, no. 2, pp. 1462–1471, Mar. 2018.

[19] M. A. Mohammed Manaz and C.-N. Lu, "Adaptive defense plan against anticipated islanding of microgrid," *IEEE Trans. Smart Grid*, vol. 10, no. 3, pp. 3071–3080, May 2019.

[20] Y. Li and L. Fan, "Stability analysis of two parallel converters with Voltage–Current droop control," *IEEE Trans. Power Del.*, vol. 32, no. 6, pp. 2389–2397, Dec. 2017.

[21] A. Reznik, M. G. Simoes, A. Al-Durra, and S. M. Muyeen, "*LCL* filter design and performance analysis for grid-interconnected systems," *IEEE Trans. Ind. Appl.*, vol. 50, no. 2, pp. 1225–1232, Mar. 2014.

[22] R. Teodorescu, M. Liserre, and P. Rodríguez, *Grid Converters for Photovoltaic and Wind Power Systems*. Chichester, U.K.: Wiley, 2011.

[23] A. Micallef, M. Apap, C. Spiteri-Staines, and J. M. Guerrero, "Single-phase microgrid with seamless transition capabilities between modes of operation," *IEEE Trans. Smart Grid*, vol. 6, no. 6, pp. 2736–2745, Nov. 2015.

[24] Q. Fu, A. Nasiri, V. Bhavaraju, A. Solanki, T. Abdallah, and D. C. Yu, "Transition management of microgrids with high penetration of renewable energy," *IEEE Trans. Smart Grid*, vol. 5, no. 2, pp. 539–549, Mar. 2014.

[25] A. M. Gole, S. Filizadeh, R. W. Menzies, and P. L. Wilson, "Optimization-enabled electromagnetic transient simulation," *IEEE Trans. Power Del.*, vol. 20, no. 1, pp. 512–518, Jan. 2005.

[26] S. Filizadeh, A. M. Gole, D. A. Woodford, and G. D. Irwin, "An optimization-enabled electromagnetic transient simulation-based methodology for HVDC controller design," *IEEE Trans. Power Del.*, vol. 22, no. 4, pp. 2559–2566, Oct. 2007.

[27] S. Yang, Q. Lei, F. Z. Peng, and Z. Qian, "A robust control scheme for grid-connected voltage-source inverters," *IEEE Trans. Ind. Electron.*, vol. 58, no. 1, pp. 202–212, Jan. 2011.

[28] S. Moon, S.-G. Yoon, and J.-H. Park, "A new low-cost centralized MPPT controller system for multiply distributed photovoltaic power conditioning modules," *IEEE Trans. Smart Grid*, vol. 6, no. 6, pp. 2649–2658, Nov. 2015.

[29] H.-C. Chen and W.-J. Lin, "MPPT and voltage balancing control with sensing only inductor current for photovoltaic-fed, three-level, boost-type converters," *IEEE Trans. Power Electron.*, vol. 29, no. 1, pp. 29–35, Jan. 2014.

[30] Y. Shan, J. Hu, K. W. Chan, Q. Fu, and J. M. Guerrero, "Model predictive control of bidirectional DC–DC converters and AC/DC interlinking converters—A new control method for PV-wind-battery microgrids," *IEEE Trans. Sustain. Energy*, vol. 10, no. 4, pp. 1823–1833, Oct. 2019.

[31] H. Nikkhajoei and R. H. Lasseter, "Distributed generation interface to the CERTS microgrid," *IEEE Trans. Power Del.*, vol. 24, no. 3, pp. 1598–1608, Jul. 2009.

[32] N. R. Chaudhuri and B. Chaudhuri, "Considerations toward coordinated control of DFIG-based wind farms," *IEEE Trans. Power Del.*, vol. 28, no. 3, pp. 1263–1270, Jul. 2013.

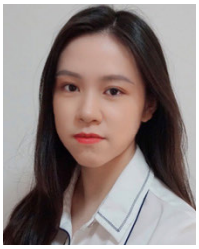

YARAN LI (Graduate Student Member, IEEE) received the B.E. degree in electrical engineering from Southeast University, Nanjing, China, in 2017. She is currently pursuing the Ph.D. degree in electrical engineering with the University of New South Wales, Sydney, NSW, Australia. She is also a Network Planning Engineer with TransGrid, Australia. Her research interests include microgrid control, renewable connection, and power system stability analysis.

LONG FU (Student Member, IEEE) received the B.E. degree (Hons.) in electrical engineering from The University of Sydney (USYD), Australia, in 2017, and the B.E. degree in electrical engineering from Beijing Jiao Tong University (BJTU), China, in 2017. He is currently pursuing the Ph.D. degree in electrical engineering with the University of New South Wales (UNSW), Sydney, NSW, Australia. His research interests include distribution network reliability and resilience, microgrids, and mixed-integer programming and its applications in power systems.

KE MENG (Senior Member, IEEE) received the Ph.D. degree in electrical engineering from The University of Queensland, Brisbane, QLD, Australia, in 2009. He is currently a Senior Lecturer with the School of Electrical Engineering and Telecommunications, University of New South Wales, Sydney, NSW, Australia. His research interests include electric power system modeling, stability analysis, renewable energy systems, and grid integration.

ZHAO YANG DONG (Fellow, IEEE) is currently a Professor of energy systems with the University of New South Wales (UNSW), Australia. He is the Director of the UNSW Digital Grid Futures Institute and the ARC Research Hub for Integrated Energy Storage Solutions. His research interests include power system planning, load modeling, smart grid/microgrid, energy market, renewable energy and its grid connection, and computational methods and their application in power system analysis. He has been serving as an editor of the several IEEE TRANSACTIONS and IET journals.

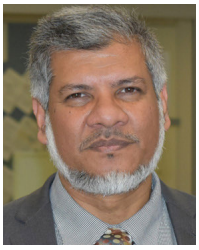

KASHEM MUTTAQI (Senior Member, IEEE) received the B.Sc. degree in electrical and electronic engineering from the Bangladesh University of Engineering and Technology (BUET), Dhaka, Bangladesh, in 1993, the M.Eng.Sc. degree in electrical engineering from the University of Malaya, Kuala Lumpur, Malaysia, in 1996, and the Ph.D. degree in electrical engineering from Multimedia University, Selangor, Malaysia, in 2001. He worked as a Lecturer with Multimedia University for a period of three years. From 2000 to 2002, he was a Research Fellow with the Queensland University of Technology, Brisbane, QLD, Australia. From 2002 to 2007, he was a Research Fellow/Lecturer/Senior Lecturer with the University of Tasmania, Hobart, TAS, Australia. He is currently a Professor with the School of Electrical, Computer, and Telecommunications Engineering, University of Wollongong, Wollongong, NSW, Australia. He has more than 22 years of academic experience. He has authored or coauthored 365 papers in international journals and conference proceedings. His research interests include distributed generation, renewable energy, electrical vehicles, smart-grid, and power system planning and control.

WENLI DU received the B.Sc. and M.Sc. degrees in chemical process automation from the Dalian University of Technology, Dalian, China, in 1997 and 2000, respectively, and the Ph.D. degree in control theory and control engineering from the East China University of Science and Technology, Shanghai, China, in 2005.

She is currently a Professor and the Dean of the College of Information Science and Engineering and the Vice Dean of the Key Laboratory of Advanced Control and Optimization for Chemical Process, Ministry of Education, East China University of Science and Technology. Her current research interests include control theory and applications, system modeling, advanced control, and process optimization.